Co:CdS Diluted Magnetic Semiconductor Nanoparticles: Radiation Synthesis, Dopant−Defect Complex Formation, and Unexpected Magnetism

Kashinath A. Bogle,[†] Saurabh Ghosh,[‡] Sanjay D. Dhole,[†] Vasant N. Bhoraskar,[†] Lian-feng Fu,[§] Miao-fang Chi,[§] Nigel D. Browning,[§] Darshan Kundaliya,[||] Gour P. Das,[‡] and Satishchandra B. Ogale*,[⊥]

Physical and Materials Chemistry Division, National Chemical Laboratory, Pune 411008, India, Department of Physics, University of Pune, Pune 411007, India, Indian Association for the Cultivation of Science, Kolkata 700032, India, Department of Chemical Engineering and Materials Science, University of California, Davis, California 95616, National Center for Electron Microscopy, MS 72-150, Lawrence Berkeley National Laboratory, Berkeley, California 94720, and Center for Superconductivity Research, University of Maryland, College Park, Maryland 20742

Received July 31, 2007

Incorporating a dopant into a nanoparticle is a nontrivial proposition in view of the size dependent surface versus bulk energy considerations and the intrinsic proximity of the surface to the interior, which facilitates migration to the surface. If realized and controlled, however, it can open up new avenues to novel nanomaterials. Some previous studies have shown the dopability of nanosystems but only with specific surface functionalization. Here, we demonstrate the successful dopant incorporation via a new route of pulsed high energy electron induced synthesis. We choose a system Co:CdS (dilutely cobalt doped cadmium sulfide) in view of the well-known application-worthy properties of CdS and the potential possibility of its conversion to a diluted magnetic semiconductor of interest to spintronics. By using various techniques, we show that matrix incorporation and uniform distribution of cobalt are realized in CdS nanocrystals without the need for additional chemical or physical manipulation. Optical and photoluminescence properties also support dopant incorporation. Interestingly, although magnetism is realized, it is weak, and it decreases at higher cobalt concentration. First principle density functional calculations are performed to understand this counterintuitive behavior. These calculations suggest that the introduction of parent cation or anion vacancies lead to magnetic moment reduction, albeit marginally. However, with some Co impurity fraction in the octahedral interstitial site inside the wurtzite cage, the magnetic moment drops down drastically. This study reveals that defect states may have an interesting role in dopant stabilization in nanosystems, with interesting system dependent consequences for the properties.

Introduction

The introduction and management of dopants and defects in solids have always been a problem of central importance to materials science in view of their implications for device science and technology. With the emergence of nanoscience and related novel device concepts, the same issue is now acquiring renewed significance. However, because of the inherent proximity of a surface in any nanosystem and the potential role of any surface as a sink for defects and a chemical asperity such as a dopant, this problem is nontrivial in such systems.[1–7] Indeed, studies have shown that the specificity of the structure, chemistry, and surface chemistry (as controlled by capping or ambient conditions) collectively define the energetics and stability of dopants and defects in nanosystems. This also highlights the importance of the growth method (equilibrium vs nonequilibrium) in achieving a particular state of a nanomaterial with incorporated dopants and defects. Some recent insightful studies[6,7] have begun to address these issues, especially in the context of magnetic dopant incorporation into semiconductor matrixes, to realize new spintronics materials such as diluted magnetic semiconductors (DMS). The DMS field has evolved to be quite interesting but controversial in recent years as a result of matters related to the uniformity of dopant incorporation and

* Corresponding author. Phone: +91-20-25902260. Fax: +91-20-25902636. E-mail: sb.ogale@ncl.res.in.
[†] University of Pune.
[‡] Indian Association for the Cultivation of Science.
[§] University of California.
[||] University of Maryland.
[⊥] National Chemical Laboratory.

(1) Mikulec, F. V.; Kuno, M.; Bennati, M.; Hall, D. A.; Griffin, R. G.; Bawendi, M. G. *J. Am. Chem. Soc.* **2000**, *122*, 2532.
(2) Dalpian, G. M.; Chelikowsky, J. R. *Phys. Rev. Lett.* **2006**, *96*, 226802 and references therein.
(3) Venkatesan, M.; Fitzgerald, C. B.; Coey, J. M. D. *Nature* **2004**, *430*, 630.
(4) Osorio-Guillén, J.; Lany, S.; Barabash, S. V.; Zunger, A. *Phys. Rev. Lett.* **2006**, *96*, 107203.
(5) Shinde, S. R.; Bhagwat, A.; Patil, S. I.; Ogale, S. B.; Mehta, G. K.; Date, S. K.; Marest, G. *J. Magn. Magn. Mater.* **1998**, *186*, 3421998.
(6) Radovanovic, P. V.; Gamelin, D. R. *J. Am. Chem. Soc.* **2001**, *123*, 12207.
(7) Kittilstved, K. R.; Gamelin, D. R. *J. Am. Chem. Soc.* **2005**, *127*, 5292.

10.1021/cm702118w CCC: $40.75
Published on Web 12/19/2007

the possibilities of secondary phases and extrinsic effects.[8–16] New mechanisms of exchange interactions between dopants as well as possible defect ferromagnetism have also been proposed and searches have been made of samples with well characterized microstates for their validity or otherwise.[17,18] There have been experimental studies on the question of magnetic dopants in semiconductor nanoparticles,[19–23] but more comprehensive studies are clearly needed. Recently, Gamelin and Radovanovic[6] have shown that normal soft chemical processing does not render cobalt substitution in a CdS matrix and that the dopants are diverted to the surface. They have proposed and demonstrated an interesting isocrystalline core/shell strategy to circumvent this problem, although the dopant uniformity within the particle is not addressed. Unfortunately, no magnetic properties are examined. In this work we use the same material system (cobalt doped cadmium sulfide, Co:CdS) but a different nanosynthesis method (MeV electron irradiation of salts[24] in stoichiometric proportion in a liquid medium, please see the Experimental Section and the Supporting Information) to demonstrate the matrix incorporation of dopants without the need for additional manipulation. By combined experimental and theoretical studies, we show that defects can play a very interesting role in dopant stabilization in nanomaterials but concurrently influence their properties as well. Dopant incorporation is established by lattice parameter evolution (X-ray diffraction (XRD)) whereas dopant uniformity is brought out by scanning high resolution transmission electron microscopy (HRTEM) and electron energy loss spectroscopy (EELS). EELS and X-ray photoelectron spectroscopy (XPS) are also used to ascertain the dopant valence state. Evolution of luminescence properties with dopant concentration further supports the related findings. We have also carried out first principles density functional theory (DFT) calculations using the tight binding linear muffin-tin orbital (TB-LMTO) supercell approach[25] within the local spin density approximation (LSDA) to offer theoretical insights into the defect−dopant-property issues.

Experimental Section

A solution containing 10^{-2} M $CdCl_2$, 10^{-3} M CS_2, 10^{-4} M $C_4H_6CoO_4{:}H_2O$ (for Co doping), and 10^{-3} M surfactant 1-thioglycrol (for encapsulation) in ethanol was prepared and filled in thin walled glass bottles, each of height ∼25 mm and diameter ∼15 mm. An electron beam of 6 MeV energy was obtained from the Race-Track Microtron of the University of Pune. The electron beam extracted through the aluminum window of the extraction port was scattered by a thin tungsten foil kept in air. In this way, irradiation of a sample under atmospheric conditions was possible. A specially made Faraday cup was kept at a distance from the extraction port of the Race-Track Microtron such that the spot of the electron beam on the ZnS(Ag) screen of the Faraday cup could reach a diameter of ∼30 mm. One bottle at a time was mounted vertically on the ZnS(Ag) screen of the Faraday cup. In this way, the entire volume of the solution could be exposed to the incident 6 MeV electrons. Each bottle was exposed to 6 MeV electrons, and the electron fluence was measured by a current integrator coupled to the Faraday cup. After exposing the solution to a set value of the electron fluence, the machine was put off and the bottle was removed from the Faraday cup. Another sample bottle was mounted on the Faraday cup, and the solution was exposed to electrons. In this manner, a number of bottles were irradiated with 6 MeV electrons. In this experiment, the electron fluence was kept constant at 5×10^{14} e/cm^2, for which the irradiation period was ∼200 s. In the electron irradiated solution, yellow precipitates were observed even after an irradiation period of 100 s. These precipitates were collected and washed with pure ethanol and distilled water. After drying the precipitate at 50 °C, a small amount of yellow powder was obtained. In this manner, the yellow powder of pure CdS and Co:CdS was synthesized. The undoped and doped CdS samples were characterized by XRD, HRTEM, EELS, XPS, absorption spectroscopy, photoluminescence (PL), and superconducting quantum interface device techniques.

Results and Discussion

The XRD pattern presented in Figure 1a for a Co:CdS nanoparticle (NP) sample shows the expected series of reflections that can be assigned to a wurtzite structure.[24,26,27] No impurity peaks are seen. The particle size, estimated using Scherrer's formula, is about 9 ± 2 nm. A slow scan near the (002) position (Figure 1b) showed a clear peak shift toward a higher 2θ (lower d value) with increasing Co concentration, as seen in Figure 1b for the (002) and (101) plane systems. This implies lattice compression,[22] consistent with the smaller ionic radii of Co^{2+} (82 pm) or Co^{3+} (64 pm) than of Cd^{2+} (103 pm),[28] strongly indicating the desired dopant incorporation. Here we mention both valence states,

(8) Prellier, W.; Fouchet, A.; Mercey, B. *J. Phys.: Condens. Matter* **2003**, *15*, R1583.
(9) Pearton, S. J.; Heo, W. H.; Ivill, M.; Norton, D. P.; Steiner, T. *Semicond. Sci. Technol.* **2004**, *19*, R59.
(10) Zutic, I.; Fabian, J.; Sarma, S. D. *Rev. Mod. Phys.* **2004**, *76*, 323.
(11) MacDonald, A. H.; Schiffer, P.; Samarth, N. *Nat. Mater.* **2005**, *4*, 195.
(12) Ogale, S. B. *Thin Films and Heterostructures for Oxide Electronics*; Springer Verlag: Berlin, 2005.
(13) Kim, J. Y.; Park, J. H.; Park, B. G.; Noh, H. J.; Oh, S. J.; Yang, J. S.; Kim, D. H.; Bu, S. D.; Noh, T. W.; Lin, H. J.; Hsieh, H. H.; Chen, C. T. *Phys. Rev. Lett.* **2003**, *90*, 17401.
(14) Shinde, S. R.; Ogale, S. B.; Higgins, J. S.; Zheng, H.; Mills, A. J.; Kulkarni, V. N.; Ramesh, R.; Greene, R.; Venkatesan, T. *Phys. Rev. Lett.* **2004**, *92*, 166601.
(15) Kundaliya, D. C.; Ogale, S. B.; Lofland, S. E.; Dhar, S.; Metting, C. J.; Shinde, S. R.; Ma, Z.; Verughese, B.; Ramanujachary, K. V.; Salamanca-Riba, L.; Venkatesan, T. *Nat. Mater.* **2004**, *3*, 709.
(16) Ogale, S. B.; Choudhary, R. J.; Buban, J. P.; Lofland, S. E.; Shinde, S. R.; Kale, S. N.; Kulkarni, V. N.; Higgins, J.; Lanci, C.; Simpson, J. R.; Browning, N. D.; Das Sarma, S.; Drew, H. D.; Greene, R. L.; Venkatesan, T. *Phys. Rev. Lett.* **2003**, *91*, 77205-1.
(17) Kaminski, A.; Das Sarma, S. *Phys. Rev. Lett.* **2002**, *88*, 247202.
(18) Coey, J. M. D.; Venkatesan, M.; Fitzgerald, C. B. *Nat. Mater.* **2005**, *4*, 173.
(19) Counio, G.; Esnouf, S.; Gacoin, T.; Boilot, J. P. *J. Phys. Chem.* **1996**, *100*, 20021.
(20) Levy, L.; Hochepied, J. F.; Pileni, M. P. *J. Phys. Chem.* **1996**, *100*, 18322.
(21) Feltin, N.; Levy, L.; Ingert, D.; Pileni, M. P. *Adv. Mater.* **1999**, *11*, 398.
(22) Hanif, K. M.; Meulenberg, R. W.; Strouse, G. F. *J. Am. Chem. Soc.* **2002**, *124*, 11495.
(23) Erwin, S. C.; Zu, L.; Haftel, M. I.; Efros, A. L.; Kennedy, T. A.; Norris, D. J. *Nature* **2005**, *436/7*, 91.
(24) Bogle, K. A.; Dhole, S. D.; Bhoraskar, V. N. *Radiat. Eff. Defects Solids* **2004**, *159*, 157.
(25) Anderson, O. K.; Jepsen, O.; Sob, M. In *Electronic Band Structure and its Applications*; Yussouff, M., Ed.; Springer: Heidelberg, 1987; p 1.
(26) Ge, X.; Ni, Y.; Zhang, Z. *Radiat. Phys. Chem.* **2002**, *64*, 223.
(27) Patil, L. A.; Wani, P. A. *Cryst. Res. Technol.* **2001**, *36*, 371.
(28) Emsley, J. *The Elements*; Clarendon Press: Oxford, 1998.

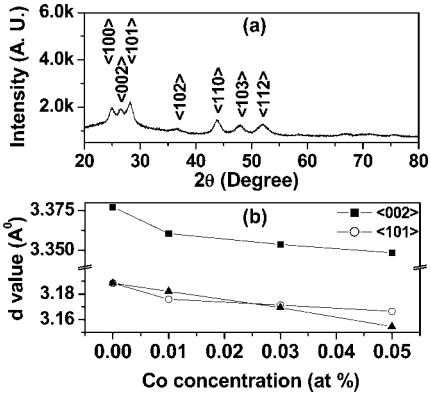

Figure 1. (a) XRD pattern for a Co:CdS (5 atom % Co) sample and (b) shift in the *d* values for the (002) and (101) plane systems as a function of doped cobalt concentration. The shift for the (101) case as expected from Vegard's law is shown by the ▲ curve.

both being smaller ions than Cd^{2+}, because we address the valence issue later in the text. The nonsaturation of the lattice relaxation implies that cobalt is incorporated in the lattice (causing lattice distortion) even up to the maximum concentration of 5 atom % studied in this work. However, it should be noted that the rate of reduction of the lattice parameter is slower at a concentration greater than ~1%. The expected nature of the lattice parameter variation by applying Vegard's law[29] to the mixed state of CdS and $Co_{1-x}S$ (JCPDS card PDF no. 42-0826) and by normalizing at the value for the undoped case is also shown in Figure 1b. The observed trend does not exactly follow the experimental data, although the order of magnitude of the change is reasonable and in the right direction. The precise valence state of cobalt and its lattice location as well as the possible presence of a defect would together control the precise nature of this dependence, and the similarity of the trends can only be expected to be nominal. At a concentration above ~1%, the change in slope may signify some change in these states with increased cobalt concentration.

The transmission electron microscopy (TEM) micrograph of the Co:CdS NPs is shown in Figure 2a, whereas the corresponding HRTEM micrograph is shown in Figure 2b. The low resolution micrograph establishes the reasonable uniformity of the particle size, and the HRTEM image reveals that the nanocrystals are faceted, crystalline, and of average size of ~9 nm. The Co−L_2 and Co−L_3 EELS spectra recorded on a typical single isolated nanocrystal at an energy resolution of 0.6 eV (beam size of 0.2 nm) at three different positions are shown in Figure 2c. These EELS spectra show a Cd−M_3 signal at 616 eV and strong Co−L_3 and Co−L_2 edges at 779 and 794 eV, respectively. Note that the Cd signal in this energy range is M_3; hence, it is small in intensity. These results confirm the formation of the Co:CdS NPs and establish a fair degree of uniformity of the cobalt distribution across the nanocrystal. It is clear that any cobalt metal cluster is neither seen by the HRTEM nor sensed in the form of a disproportionately strong local Co−EELS signal. A similar condition was encountered in other nanocrystals in the same sample. One could argue that a fairly

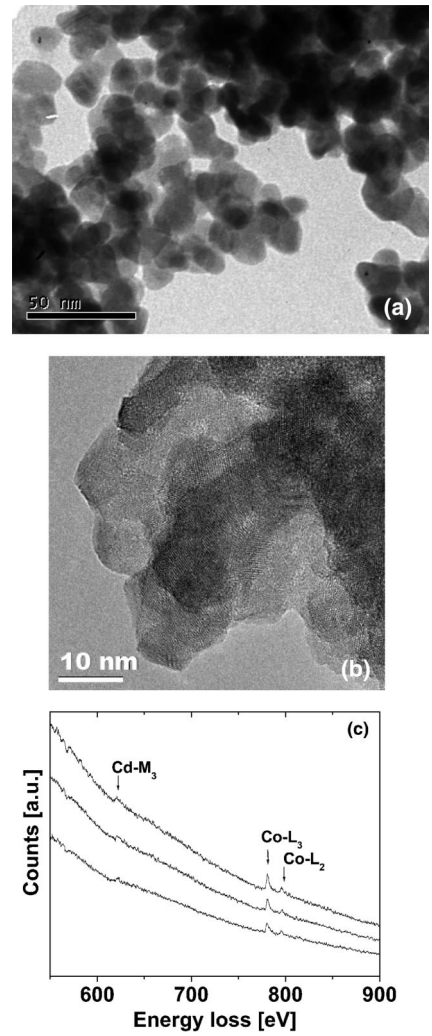

Figure 2. (a) TEM image for Co:CdS NPs, (b) HRTEM image, and (c) EELS for the edge−center−edge of a single Co:CdS NP.

uniform EELS signal could be encountered even if all the cobalt lies on the surface of the faceted NPs. However, in this case a systematic change will not be seen in the XRD *d* parameters, as observed and depicted in Figure 1. Small differences between different EELS scan intensities could arise because of several reasons in this high resolution experiment. For instance, the specific shape of a NP being examined will dictate the cumulative dopant contribution across the penetration depth. It may suffice to state here with confidence that no gross structural or dopant concentration inhomogeneties are seen in the state of the sample.

The Co valence state measurement from the Co−$L_{2,3}$ white line edges gives the mean valence to be ~3.1^+. This analysis was based on the calculation of the intensity ratio of the Co−L_3 and Co−L_2 edges and its comparison with the ratio map provided by Wang et al.[30] as shown in Figure 3. To subtract the normalized white line ratio, we followed the same procedure as the one described in Wang et al.'s paper. Although there could be some uncertainties in this estimate as a result of the small intensity of the cobalt signal, it can be definitely stated that the valence is certainly not Co(0)-

(29) Denton, A. R.; Ashcroft, N. W. *Phys. Rev. A* **1991**, *43*, 3161.

(30) Wang, Z. L.; Yin, J. S.; Jiang, Y. D. *Micron* **2000**, *31*, 571.

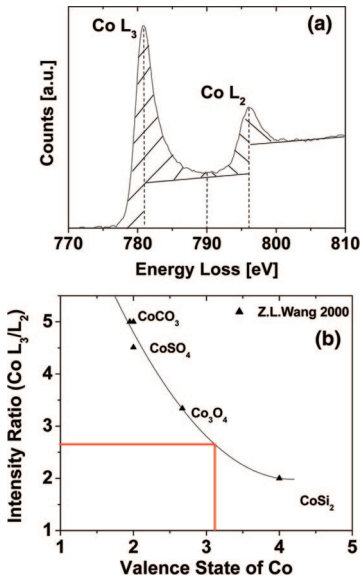

Figure 3. (a) Magnified spectra from Co−L_2 and Co−L_3 lines and (b) the Co valence state measurement based on the calculation of intensity ratio of Co−L_3 and Co−L_2 edges (~3.1^+ (±0.2)).

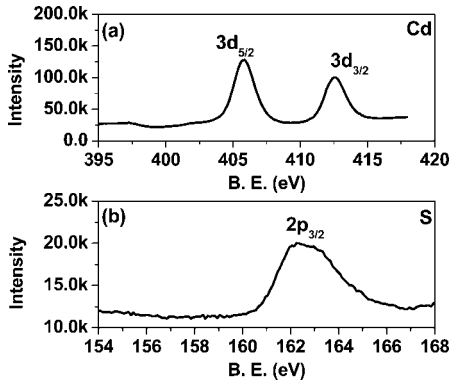

Figure 4. XPS spectra for (a) Cd $3d_{5/2}$ and $3d_{3/2}$ and (b) S $2p_{3/2}$ in the undoped CdS NP sample.

like as it is for the cobalt metal. Thus, the experimental condition employed for the synthesis does not appear to lead to cobalt metal cluster formation.

The XPS spectra for the undoped CdS NPs synthesized by 6 MeV electron irradiation are shown in Figure 4a,b. In this case, the Cd $3d_{5/2}$, Cd $3d_{3/2}$, and S $2p_{3/2}$ contributions are noted at binding energies of 405.75, 412.55, and 162.65 eV, respectively. From these, the S $2p_{3/2}$ is found to be blue-shifted when compared with that of the standard CdS, which varies from 161.4 to 162.2 eV.[31–33] This may indicate the presence of defect contributions and related strains. In the case of the radiation synthesized Co:CdS NP sample, the XPS peaks in Figure 5a,b clearly show the Cd $3d_{5/2}$, Cd $3d_{3/2}$, and S $2p_{3/2}$ contributions at the binding energies of 405.95, 412.65, and 163.25 eV, respectively (Table 1). The Cd 3d peaks are found to be slightly blue-shifted, 0.2 and 0.1 eV, from those of the undoped CdS NPs; however, the S $2p_{3/2}$ contribution is even further blue-shifted. This would suggest an interaction

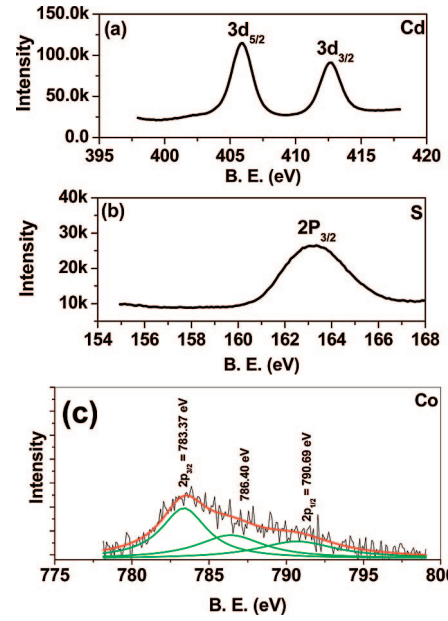

Figure 5. XPS spectra for (a) Cd $3d_{5/2}$ and $3d_{3/2}$, (b) S $2p_{3/2}$, and (c) Co $2p_{3/2}$ and $2p_{1/2}$ in the Co:CdS NP sample.

Table 1. XPS Energies

series no.	species present	pure species	CdS standard	radiation synthesized CdS	radiation synthesized Co:CdS
1	C 1s			285.15 eV	285.15 eV
2	O 1s			532.55 eV	532.55 eV
3	S $2p_{3/2}$	163.1−164.8 eV	161.4−162.2 eV	162.65 eV	163.25 eV
4	Cd $3d_{5/2}$	404.6−405.3 eV	405.1−405.5 eV	405.75 eV	405.95 eV
5	Cd $3d_{3/2}$			412.55 eV	412.65 eV

between the doped cobalt and the intrinsic defects formed as a result of the nonequilibrium nature of this process. As we will discuss later, these aspects have an important bearing on the evolution of the physical properties.

Figure 5c shows the Co 2p XPS spectrum of the Co:CdS for a Co concentration of 3 atom %. As a result of the low dopant concentration, the signal-to-noise ratio is rather low. In this case, the Co $2p_{3/2}$ binding energy is observed at 783.37 eV. If the NPs had cobalt in metallic form (Co(0)), the binding energy for $2p_{3/2}$ should have appeared at 778.1 eV, and if cobalt were in the Co^{2+} state, it should have appeared at 781.5 eV.[34,35] Generally, the core level binding energy increases with increasing positive valence of the ion.[36] Thus, the observed blue shift in the Co $2p_{3/2}$ peak in our sample may imply a higher valence state. Moreover, the other fitted contributions in Figure 5c suggest a complex environment for the doped cobalt.

Figure 6 compares the UV–vis absorption spectra for the CdS NPs without and with Co doping at various concentrations. The presence of the absorption peak at ~422 nm is

(31) Marychurch, M.; Morris, G. C. *Surf. Sci.* **1985**, *154*, L251.
(32) Bhide, V. G.; Salkalachan, S.; Rastogi, A. C.; Rao, C. N. R.; Hedge, M. S. *J. Phys. D* **1981**, *14*, 1647.
(33) Houng, M. P.; Fu, S. L.; Wu, T. S. *J. Mater. Sci.* **1986**, *5*, 96.
(34) Wagner, C. D.; Rigg, W. M.; Davis, L. E.; Moulder, J. F.; Muilenberg, G. F. *Handbook of X-ray Photoelectron Spectroscopy*; Perkin-Elmer Corporation, Physical Electronic Division: Eden Prairie, MN, 1979; p 55344.
(35) Tan, B. J.; Klabunde, K. J.; Sherwood, P. M. A. *J. Am. Chem. Soc.* **1991**, *113*, 855.
(36) Hufner, S. *Photoelectron Spectroscopy, Principles and Applications*; Springer-Verlag: Berlin, 2003.

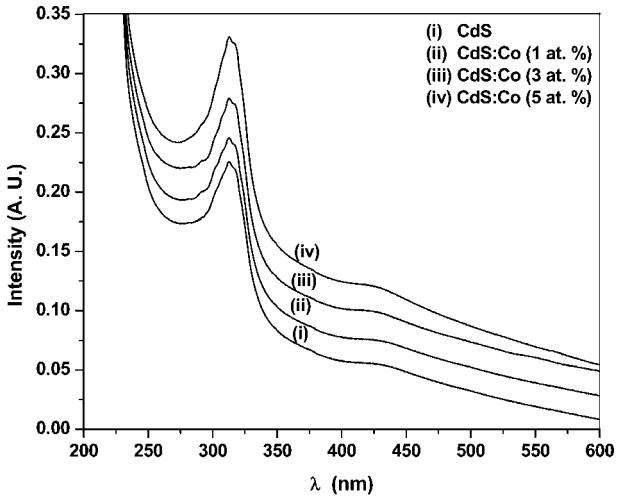

Figure 6. The UV–vis absorption spectra for the CdS NPs without and with Co doping at various concentrations.

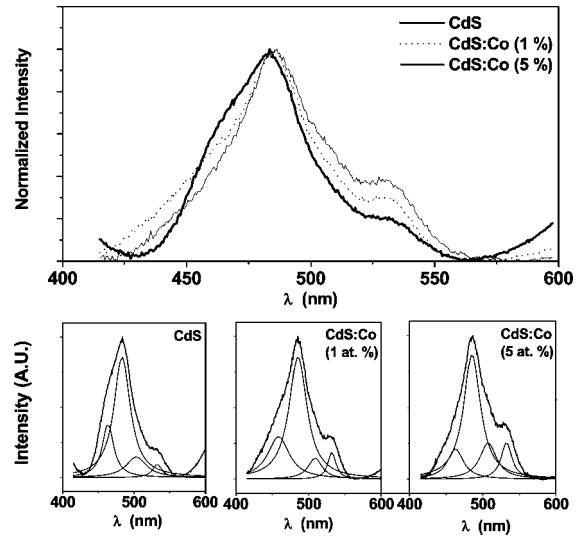

Figure 7. PL spectra for the CdS NPs without and with Co doping at 1 atom % and 5 atom %.

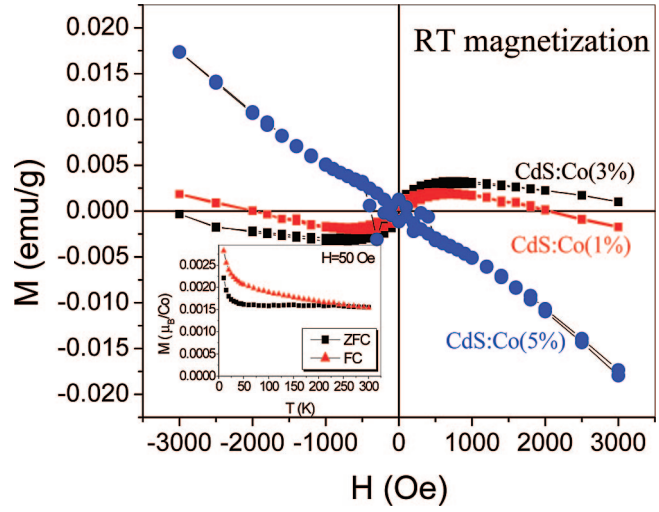

Figure 8. *M* vs *H* loop of Co:CdS NPs at room temperature for 1, 3, and 5 atom % Co. Inset shows the FC/ZFC *M* vs *T* data for the Co:CdS (1 atom %) NPs.

attributed to the characteristic absorption band edge of the CdS NPs, which is blue-shifted from that of the corresponding bulk band gap (2.4 eV) of CdS,[37,38] as expected. Additionally, a strong peak at 306 nm is observed, which indicates the presence of extremely tiny sized CdS nanoclusters (NCs).[39,40] Thus, the sample appears to have a bimodal size distribution. These tiny NCs do not settle down easily in centrifugation and isolation procedures; hence, the rest of the measurements basically correspond to the ~9 nm NPs. This can possibly be attributed to the irradiation synthesis process whereby, in an equilibrium condition, extremely tiny CdS NCs dynamically form by disintegration. It is interesting to note that the absorption peak for the Co:CdS NPs appears nearly at the same position (~422 nm) with a noticeable increase in the peak intensity. Thus, the incorporation of Co atoms in the CdS lattice does not alter the absorption edge of the NPs significantly. A similar observation has been reported earlier for Mn doping in CdS.[41] The average diameter of the NPs is estimated to be ~9 nm from the effective mass approximation.[42] This is consistent with the size estimate by XRD and TEM measurements.

The PL (Figure 7) spectrum of undoped CdS excited at $\lambda_{ex} = 358$ nm shows strong luminescence peaks at 466 and 483 nm and two weak/broad peaks at 504 and 531 nm. In soft chemically prepared CdS NPs, the observed PL is less complex,[43,44] suggesting that in our case some forms of defects may be present in the NPs. The strong peaks at 466 and 483 nm, which are closer to the band edge (422 nm), can then be attributed to bound excitonic luminescence; the two contributions possibly arise from two different binding defect centers. The smaller contributions at 504 and 531 nm could be due to deep level states. Indeed, a contribution near 530 nm has been previously reported and attributed to midgap surface states.[43]

In the case of Co:CdS NPs, the overall PL structure appears over the same wavelength range, although the weight of different contributions is seen to change. The PL peak at 483 nm seems to be largely unaffected. The contribution near 466 nm is gradually suppressed and broadened. Interestingly, the gross contribution in the region near 530 nm appears to grow systematically with increase in cobalt concentration. It seems therefore that the cobalt contribution overlaps with the intrinsic defect/surface luminescence of the CdS NPs.

The Co:CdS NPs are found to be ferromagnetic (FM, Figure 8), although apparently with a weak magnetic moment. The actual moment per cobalt may be higher but

(37) Ni, Y.; Ge, X.; Liu, H.; Xu, X.; Zhang, Z. *Radiat. Phys. Chem.* **2001**, *61*, 61.
(38) Liu, S. M.; Liu, F. Q.; Guo, H. Q.; Zhang, Z. H.; Wang, Z. G. *Solid State Commun.* **2000**, *115*, 615.
(39) Chen, W.; Lin, Z.; Wang, Z.; Lin, L. *Solid State Commun.* **1996**, *100*, 101.
(40) Vossmeyer, T.; Katsikas, L.; Giersig, M.; Popovic, I. G.; Diesner, K.; Chemseddine, A.; Eychmuller, A.; Weller, H. *J. Phys. Chem.* **1994**, *98*, 7665.
(41) Corrí, C. B.; Remenyi, C.; Dem, C.; Schmitt, M.; Kiefer, W.; Gould, C.; Ruster, C.; Schmidt, G.; Hofmann, D. M.; Pfisterer, D.; Muller, G. *Phys. Chem. Chem. Phys.* **2003**, *5*, 1639.
(42) Brus, L. *J. Chem. Phys.* **2000**, *8*, 174.
(43) Cao, H.; Wang, G.; Zhang, S.; Zhang, X.; Rabinovich, D. *Inorg. Chem.* **2006**, *45*, 5103.
(44) Wang, Y.; Sung, A.; McHugh, J.; Hilinski, E. F.; Lucas, P. A.; Johnson, R. D. *J. Chem. Phys.* **1990**, *92*, 6927.

cannot be ascertained easily because of the difficulty in subtracting the unknown diamagnetic contribution of CdS and the unaccounted weight of the molecular dressing, which was provided for dispersion. Heating the NPs to remove the dressing also sinters and modifies them; hence, heating was not done. Small values of the moment have been reported earlier in NP aggregates[45] and have been attributed to increased domain volumes and to the introduction of donor type defects. Although weak, this FM behavior is clearly of fundamental importance. Remarkably, this value of the moment drops with increasing Co concentration, as seen in some other systems and suggesting new operative mechanisms of FM behavior.[17,18] It may be noted that the rise in the actual moment (emu/g) with increase in cobalt concentration from 1% to 3% is very small; hence, the moment per cobalt would decrease as the Co concentration increases from 1% to 3%. For 5%, it is, in fact, negligible. The inset reflects the field cooled (FC) and zero field cooled (ZFC) magnetization reflecting a blocking temperature of ~280 K. The small opening of the loop at 300 K in hysteresis possibly represents the cooperative interactions in the particle assembly.

Given the semiconducting nature of CdS and the large radius of an excitonic state (~2.8 nm), one could seek the origin of FM behavior in the percolation model proposed by Kaminski and Das Sarma[17] and Coey et al.[18] The observed moment reduction with Co concentration also appears to be consistent with this model. Whereas the observation of FM behavior may be consistent with these models, the strength of the moment clearly invites further theoretical insights, especially on issues related to the concurrent presence of defects and their influence. To understand this counterintuitive nature of ferromagnetism, the following relevant issues were addressed theoretically using first principles DFT calculations:

(a) Do Co ions (really) get distributed in the CdS lattice, or do they go to the surface, as indicated by some of the recent experiments?

(b) Does Co:CdS exhibit half-metallic behavior, and what are the possible valence states of the Co ion?

(c) Assuming that Co does get incorporated into the lattice, as the present experimental synthesis route suggests, does it go into the Cd substitutional or interstitial site? Correspondingly, what are the total, local, and induced magnetic moments?

(d) And finally, the most critical questions in the present context are as follows: Why is the experimental magnetic moment per Co atom apparently weak, and why does it drop down further with increasing Co concentration? Do vacancies (that are quite likely to be produced during the ion irradiation process) play a role in "driving down" the magnetic moment?

We have carried out first principles DFT calculations using the TB-LMTO supercell approach[25] within the LSDA method; the Vosko−Wilk−Nusair local exchange correlation potential[46] has been used along with the Perdew–Wang nonlocal corrections.[47] Nonmagnetic (NM), FM, and antiferromagnetic (AFM) calculations have been carried out on a 32-atom supercell in a wurtzite structure, with Co in the Cd-substitutional position (Co_{Cd}) or in the interstitial position inside the hexagonal wurtzite cage (Co_I). Co^{2+} ions having smaller ionic radii correspond to Cd^{2+}. Both substitutional and interstitial doping leads to shrinkage in lattice volume as observed experimentally.[46]

Table 2. Magnetic Moment (in μ_B) in Different Sites of Co:CdS without Any Vacancy, with Vacancy, and with Cd Vacancy

	without vacancy		with S vacancy		with Cd vacancy	
site	FM	AFM	FM	AFM	FM	AFM
Co1	2.421	−2.380	2.380	−2.370	2.537	−2.490
Co2	2.422	2.380	2.400	2.340	2.517	2.488
Cd (1NN of Co1 and Co2)	0.012	−0.002	0.010	−0.002	0.022	−0.004
Cd (1NN of Co1)	0.005	−0.004	0.004	−0.004	0.013	−0.010
Cd (1NN of Co2)	0.005	0.002	0.015	0.002	0.007	−0.004
S (1NN of Co1 and Co2)	0.182	−0.004	0.150	−0.010	0.250	0.000
S (1NN of Co1)	0.105	−0.102	0.091	−0.080	0.150	−0.140
S (1NN of Co2)	0.103	0.102	0.096	0.080	0.154	0.136
total	6.000	0.000	5.870	0.000	6.853	0.006

Whereas the technical details of our calculations will be published elsewhere, here we focus mainly on the magnetic behavior of the Co:CdS system. We have carried out five sets of calculations:

12.5% Co_{Cd} doped CdS without vacancy

12.5% Co_{Cd} doped CdS with 6.25% S-vacancy (n-type doping)

12.5% Co_{Cd} doped with 6.25% Cd-vacancy (p-type doping)

6.25% Co_I doped CdS without vacancy

6.25% Co_I and 6.25% Co_{Cd} doped CdS without vacancy

Our overall findings can be summarized as follows:

(a) With two Co atoms selectively replacing Cd in a CdS host lattice (supercell formula unit $Cd_{14}Co_{Cd2}S_{16}$), the nonspin polarized density of states (DOS) shows deep Co d-derived states in the semiconducting gap of CdS, which are broadened as a result of hybridization with S p-states. The resulting high DOS (not shown) at the Fermi level implies that, with Co doping, the paramagnetic ground state becomes unstable, which can be stabilized by introducing a spin polarization that separates the spin up and spin down electrons energetically.

Our spin-polarized results, in fact, show some substantial reduction (by ~854 meV) of the total energy with respect to the NM state and manifests 100% spin splitting, that is, half-metallic behavior. The valence state of Co can be either Co^{2+} or Co^{3+} in a cation substitutional case, thereby making it a d^7 or d^6 state, respectively. For a Co atom in a tetrahedral coordination, the crystal field splitting ensures a 3-fold degenerate t_2 level above the 2-fold degenerate e level, and the system favors a high spin configuration via $e^{\downarrow}(2)t_2^{\downarrow}(3)e^{\uparrow}(2)t_2^{\uparrow}(0)$; that is, the majority spin channel (spin down) is completely filled.

We have carried out supercell calculations for both the FM and AFM configurations for the Co ions, and we find that the FM configuration is lower in energy by ~34 meV

(45) Bryan, J. D.; Heald, S. M.; Chambers, S. A.; Gamelin, D. R. *J. Am. Chem. Soc.* **2004**, *126*, 11640.

(46) Vosko, S. H.; Wilks, L.; Nusair, M. *Can. J. Phys.* **1980**, *58*, 1200.

(47) Perdew, J. P.; Wang, Y. *Phys. Rev. B* **1986**, *33*, 8800.

Table 3. Magnetic Moment (in μ_B) on a Co Site When Co Is in (A) an Interstitial Site Only and (B) along with Co in a Substitutional Site

site	Co_I	Co_{Cd}
(A) Co in interstitial position	0.960	
(B) Co in both interstitial and substitutional position	0.924	0.924

per Co. The spin polarized DOS's clearly showed that the Co 3d ↑ peaks lie right inside the local density band gap of CdS and above the valence band top, whereas the down spin DOS at Fermi level is zero. With two Co atoms at the first nearest neighbor sites (Co−Co distance 4.121 Å), the total magnetic moment is 3 μ_B per Co atom, which is contributed predominantly by the local magnetic moment of Co (2.42 μ_B) and the induced moments on the neighboring Cd and S sites [Table 2].These values of the magnetic moment are in sharp contrast to those observed experimentally. To underscore this discrepancy, we have carried out self-consistent calculations by introducing anion as well as cation vacancies at different distances from the Co ion.

(b) In our supercell calculation, vacancies have been simulated by replacing the S/Cd atoms by empty spheres with the same radii located at different distances from the Co atom. The supercells corresponding to 6.25% S and Cd vacancies (denoted as V_S or V_{Cd}) are $Cd_{14}Co_{Cd2}S_{15}V_{S1}$ and $Cd_{13}Co_{Cd2}S_{16}V_{Cd1}$, respectively. In either case, the FM configuration turns out to be lower in energy compared to the AFM configuration. The corresponding spin polarized DOS clearly showed that for the S vacancy the system remains half-metallic. The minority Co-d band (spin up) shifts toward lower energy. On other hand, for the Cd vacancy the system becomes metallic and the minority Co-d band (spin up) shifts upward.

The magnetic moment per Co atom reduces for an n-type vacancy (S vacancy) and increases for a p-type vacancy (Cd vacancy). Although we observe a shift in the magnetic moment toward the lower side for an S vacancy, the magnitude of the reduction is rather small as compared to that observed experimentally. This leads us to the speculation that the Co goes to the interstitial site as well.

(c) To simulate interstitial Co in the CdS matrix, we have carried out self-consistent calculations on $Cd_{16}Co_IS_{16}$ (corresponding to 6.25% Co:CdS). The FM state is lower in energy by ∼139 meV per Co atom than the corresponding NM state. The corresponding DOS showed some significant deviation from the substitutional case, with both the majority (spin down) and the minority (spin up) Co-d pronounced peaks lying within the CdS band gap; the Fermi level falls at the t_{2g} peak at the minority spin whereas the majority spin shows a clear band gap. That is, the spin down (majority carriers) states are completely occupied, and the spin up states (minority carriers) are partially empty. It is interesting to note the drastic reduction in magnetic moment per Co atom [Table 3] from 2.42 μ_B per Co atom in the substitutional case to 0.96 μ_B in the interstitial case. The spectral weight of the majority spins DOS shifts toward the Fermi level with a concomitant reduction in the bandwidth. Thus, our first principle DFT calculation indicates the possibility of a Co atom impurity going to an interstitial wurtzite site over an above substitutional Co atom with possible S vacancies that are formed during the ion irradiation process.

(d) Next, we consider the case of a substitutional Co_{Cd} along with another interstitial Co_I atom in the neighboring octahedral interstitial site (Co_I-Co_{Cd} distance 1.831 Å). The corresponding supercell formula unit becomes $Cd_{15}Co_ICo_{Cd1}S_{16}$.

For this situation the magnetic moment of the Co_{Cd} site and the Co_I site are both reduced to a value of 0.924 μ_B per Co impurity, with a low spin state as the ground state. It is interesting to note that when two Co atoms are at the nearest neighbor substitutional position, the average magnetic moment is 2.421 μ_B but, because of the presence of a Co atom impurity at the nearest interstitial site, the moment on the substitutional Co atom has significantly reduced to 0.924 μ_B (Table 3). It is found that the half-metallic behavior of the system is lost although the system retains its FM state as the ground state with an energy of ∼99 meV per Co impurity lower than in the NM state. The Fermi level falls in the gap by e_g and t_{2g} in the majority spin channel (spin down) as well as in the minority spin channel (spin up).

The fact that a larger magnetic moment is realized at a lower cobalt concentration and then it drops at a higher cobalt concentration may imply that, as the concentration of cobalt grows, an increasing fraction of the same is pushed to the interstitial site. This picture is also consistent with the observed relaxation of the lattice *d* values, which shows more change at lower concentration and a rate that tapers off at higher concentration.

Conclusions

In conclusion, nanocrystals of Co:CdS are synthesized using a high energy electron irradiation technique. It is shown that the incorporation and uniform distribution of cobalt are realized in the CdS nanocrystals without the need for additional chemical or physical manipulation. Optical and PL properties also support dopant incorporation. Interestingly, although magnetism is realized, it is weak and decreases with increasing cobalt concentration. First principle DFT calculations show that the introduction of parent ion vacancies leads to magnetic moment reduction, albeit marginally. However, with some Co impurity fraction in the octahedral interstitial site inside the wurtzite cage, the magnetic moment drops down drastically. This study reveals that defect engineering could be used to stabilize dopants into nanosystems and may have interesting system dependent consequences for the properties.

Acknowledgment. S.B.O. and G.P.D. would like to thank the BRNS (DAE) CRP spintronics program. S.B.O. would also like to thank the Department of Science and Technology, Govt. of India, for a Ramanujan Fellowship. The microscopy work was supported by the DOE (DE-AC02-05CH11231) and the NSF (DMR-0557660).

Supporting Information Available: NP formation by high energy pulsed electron beam (PDF). This material is available free of charge via the Internet at http://pubs.acs.org.

CM702118W